Macromolecules
ARTICLE

Macromolecules **2010**, *43*, 9441–9446 **9441**
DOI: 10.1021/ma101992c

Self-Diffusion of Polystyrene Solutions in Porous Acrylate-Based Monoliths Studied by ^{1}H PFG NMR

Steffen Beckert,[†] Frank Stallmach,*[,†] Rajendar Bandari,[‡] and Michael R. Buchmeiser*[,‡]

[†]*Institut für Experimentelle Physik I, Universität Leipzig, Linnéstrasse 5, D-04103 Leipzig, Germany, and* [‡]*Institut für Polymerchemie, Universität Stuttgart, Pfaffenwaldring 55, D-70550 Stuttgart, Germany*

Received August 27, 2010; Revised Manuscript Received October 6, 2010

ABSTRACT: The pulsed field gradient (PFG) nuclear magnetic resonance (NMR) method has been used to study the molecular self-diffusion of polystyrene (PS) solutions in porous acrylate-based monoliths. It was found that the characteristic concentration and molar mass dependencies of the PS self-diffusion in the solution (describable by the Zimm and Doi−Edwards models) remain unchanged in case that the self-diffusion occurred in this porous material. However, the self-diffusion coefficients of the PS were reduced in the monoliths by a constant factor, which is independent of the molar mass and the concentration. This constant factor represents the tortuosity of the porous monoliths and agrees with the reduction of the initial turnover frequency found in the ring-closing metathesis reaction of diethyl diallyl malonate catalyzed in these monoliths.

Introduction

The diffusion behavior of polymer solutions is studied for many years.[1,2] Most of the former publications concentrate on the comparison between theoretical predictions and experimental data of macromolecular bulk solutions and melts.[3−10] The existing experimental studies in this field apply techniques like forced Rayleigh scattering,[11−13] dynamic light scattering,[14−16] and neutron scattering.[17−19] An additional method represents the pulsed field gradient (PFG) nuclear magnetic resonance (NMR), which is known to provide a direct and nondestructive measurement of the diffusivity of NMR active nuclei without influencing the proceeding diffusion processes in solution as well in porous media.[20−22]

Porous monolithic polymeric materials have first been reported in the early 1990s.[23−25] They were originally designed for high-speed chromatographic separations, nevertheless, their most favorable properties also paved the way for use in other applications, e.g., as catalytic supports in bioreactors.[26] Monolithic polymeric materials ("monoliths") are characterized by a unitary porous structure with interconnected large pores and are usually synthesized within the confines of the compartment in which they are to be used at a later stage. The structure-forming matrix composed of interlinked microglobules itself may be porous or nonporous, depending on the application. The porosity and the pore size distribution can be tailored through synthesis. This is accomplished by determining both the onset of phase separation and the number of growing nuclei. The majority of monolithic polymeric materials has been prepared via thermally or UV-induced free radical polymerization of (meth)acrylates,[27,28] however, other techniques such as γ-irradiation[29] as well as various polyaddition and polycondensation based approaches have to be mentioned, too.[30−32] Apart from these synthetic approaches, the ring-opening metathesis polymerization based synthesis and functionalization of such supports has been elaborated by Buchmeiser et al.[33,34] aiming on applications in separation science,[35−45] heterogeneous catalysis,[46−52] and tissue engineering.[53] In addition, aiming on large volume monolithic devices, electron beam triggered free radical polymerization has been developed by the same group.[35,36,54−56]

The short analysis times in high-speed chromatographic separations, particularly for larger biomolecules, that are usually observed with such monoliths, are a result of the fast mass transfer between the mobile and the stationary phase. In particular, monolithic structures with no or very low micro- and mesoporosity and consequently with low specific surface areas reduce diffusion resistances to a minimum extent and thus allow for such fast separations. Though this has already been addressed theoretically at the beginning of the "monolithic era",[53,57−60] we were interested in whether the diffusion of macromolecules within monolithic materials follows (standard) diffusion laws. To mimic biomolecules with high molecular masses, e.g., proteins, we chose narrow polystyrene standards and investigated their diffusion behavior in solution. Deuterated benzene was chosen as a good polymer solvent to rule out any surface-polymer interactions such as irreversible adsorption, etc. In this example, the influence of the internal structure of porous acrylate-based monoliths on the self-diffusion of the macromolecules is investigated. For this purpose, we apply time-dependent PFG NMR measurements to study the self-diffusion of the PS molecules in solution of deuterated benzene.

Materials

Preparation of Monoliths. Trimethylolpropane triacrylate, ethyl methacrylate, 2-propanol 1-dodecanol, and toluene were purchased from Sigma-Aldrich. Toluene was dried by a MBraun SPS system. All monoliths were prepared from this chemicals as follows. Glass columns or tubes were cleaned, rinsed and sonicated in a 1:1 mixture of ethanol and acetone and dried for 2 h *in vacuo*. Glass columns were placed inside a test tube. The columns were filled with the polymerization mixture (trimethylolpropane triacrylate:ethyl methacrylate:2-propanol:1-dodecanol:toluene = 15:15:30:30:10 wt %), sealed at either side, and irradiated by an electron-beam to initiate the polymerization.

The general irradiation procedure for the electron-beam-triggered free radical polymerization-based synthesis of the monoliths proceeded as follows: The electron-beam irradiation was performed at a 10 MeV linear accelerator ELEKTRONIKA (Toriy Company, Moscow). The accelerator was operated

*To whom correspondence should be addressed E-mail: stallmac@physik.uni-leipzig.de; ipobuch@ipoc.uni-stuttgart.de.

Published on Web 10/21/2010

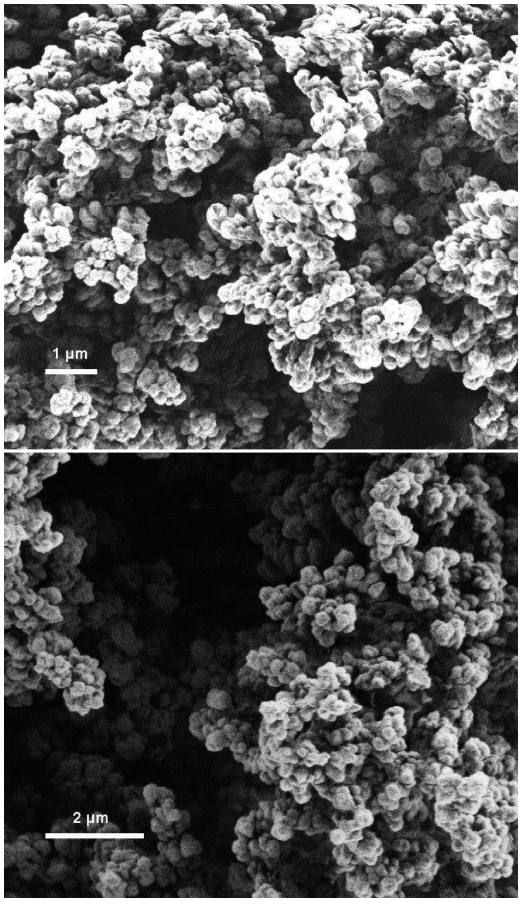

Figure 1. REM pictures of the porous acrylate-based monoliths.

at a 50 Hz repetition rate and 4 μs pulse length using a scanning horn (width up to 40 cm, scanning frequency 1 Hz) and a movable table to irradiate the samples. As a reference dose, the dose to graphite was determined with a calorimeter without further correction for the particular material irradiated. The total dose was applied incrementally in small steps (~3 kGy) over a period of 15 min in order to keep the temperature well below 50 °C. A total dose of (22 kGy) was applied. After irradiation, the glass tubes were broken to remove the monolithic rods from the glass tubes. The rods were inserted into 2 mL syringes, connected to a syringe pump and flushed with $CHCl_3$ for 4 h at a flow rate of 0.2 mL/min. After this procedure, the monoliths were ready for use and characterization.

The monolithic columns were characterized by inverse size-exclusion chromatography[61,62] as described elsewhere.[54,63] For the monoliths used in this study, the volume fraction of pores (ε_p) was 9%, the volume fraction of the interparticle void volume (ε_z) was 77%, the total porosity (ε_t) was 86% and the pore volume (V_p) of the monolith was 370 μL/g. Figure 1 shows an image of the resulting structure of the monolithic materials recorded by electron microscopy (REM) and Figure 2 showes its pore size distribution. REM was carried out on an Ultra 55 (Carl Zeiss SMT, Oberkochen, Germany).

NMR Sample Preparation. Polystyrene standards in the molecular weight range of 2600 g/mol $\leq \overline{M_{PS}} \leq$ 900 000 g/mol have been studied as solutions in deuterated benzene (C_6D_6) at concentrations c_{PS} of 2, 5, and 15 wt %. Narrow polystyrene (PS) standards with molecular masses (M_{PS}) of 2600, 17 200 g/mol were purchased from Waters (USA). In addition, polystyrene standards with molecular masses of 49 300, 62 300, 75 000, 301 600, 319 000, 524 000, 601 800, 864 000, and 900 000 g/mol were purchased from Polymer Standards Service (PSS, Mainz, Germany). All PS standards were prepared by dissolving the PS of interest in deuterated benzene.

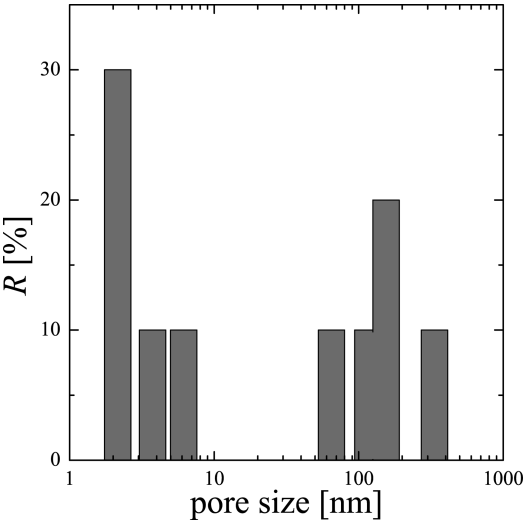

Figure 2. Pore size distribution for the porous acrylate-based monolith, where R represents the fraction of the total pore volume.

For the PFG NMR measurements, PS solutions in C_6D_6 as well as the solutions of PS in C_6D_6 soaked into the acrylate-based monoliths were inserted in glassware tubes of 7.6 mm outer diameter. Filling the accessible pores of the monoliths with the PS solution occurred by capillary action, where the lower part of the monoliths is immersed in the solution. Thus, the air could easily be replaced by the invading solution. During filling, the initially white monoliths turned opaque. Obviously, the refractive index match between the porous acrylate matrix and the PS solution reduces light scattering drastically, which is a clear indication for a homogeneous filling of the pore space. The monoliths were considered to be saturated, if they occurred homogeneously opaque. The glassware tubes were sealed immediately after preparation by melting the glass in order to prevent evaporation of the solvent.

Methods

PFG NMR. The PFG NMR technique was originally developed by Stejskal and Tanner.[64] The recorded signal is sensitive to the mean square displacement $\langle z^2(\Delta)\rangle$ of the diffusing molecules in the direction of the pulsed field gradient during the observation time Δ. Under equilibrium conditions, the mean square displacement is directly related to the self-diffusion coefficient D by the so-called Einstein relation:

$$\langle z^2(\Delta)\rangle = 2D\Delta \tag{1}$$

The PFG NMR self-diffusion measurements were carried out by means of the home-build NMR spectrometer FEGRIS NT operating at a proton resonance frequency of 125 MHz, which is equipped with a pulsed field gradient unit.[21,22,65,66] The self-diffusivities were determined by measuring the normalized attenuation $\Psi(b) \equiv M(b)/M(b = 0)$ of the NMR signal intensity as a function of the magnetic field gradient pulse strength b, the so-called b-value. The NMR signal was generated by using the Hahn echo and the stimulated echo pulse sequence with magnetic field gradient pulses as shown in Figure 3. Thereby the signal attenuation for an isotropic system obeys the relation

$$\Psi(b) = \exp(-bD) \tag{2}$$

For rectangular shaped gradients, the b-value for the used pulse sequences is given by

$$b = \gamma^2\delta^2G^2\left(\Delta - \frac{1}{3}\delta\right)$$

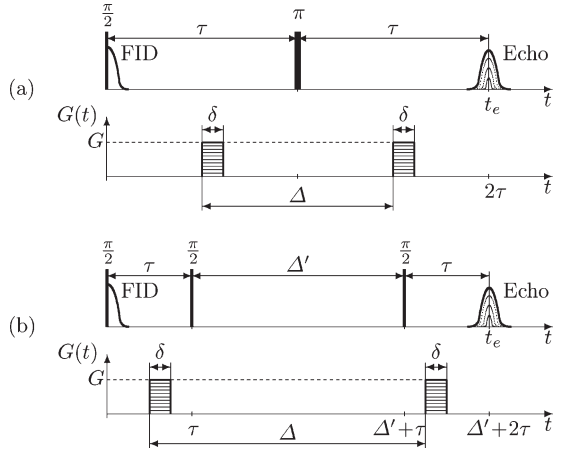

Figure 3. (a) Hahn echo and (b) stimulated spin echo sequence with pulsed field gradients $G(t)$.

with γ denoting the gyromagnetic ratio of the observed nuclei (in our case hydrogen with $\gamma = 2.67 \times 10^8\ \mathrm{T^{-1}\ s^{-1}}$), δ the magnetic field gradient width, and G the magnetic field gradient amplitude. The pulsed field gradient separation Δ represents the time scale over which the diffusion process is monitored ("observation time"). If the system contains n different phases with different self-diffusion coefficients, eq 2 becomes

$$\Psi(b) = \sum_n q_n \exp(-bD_n) \tag{3}$$

with q_n denoting the amount of molecules having the self-diffusion coefficient D_n.

In the experiments, δ was varied between 300 and 3000 μs and G was incremented up to 35.4 T/m. These values refer to the maximum of the pulsed gradient strength during the gradient pulse, which is only achieved by controlled exponentially shaped rise and fall times of the gradient currents during δ. The stability of the PFG NMR measurements under such conditions is ensured by observation of the spin echo in the time domain and adjusting its position using a small read gradient. Details of these procedures including the calculation of the b-values for such shaped gradient wave forms are extensively described by Stallmach and Galvosas[22] (sections 4.2.2 and 4.2.4). Generally, several scans were recorded to increase the signal-to-noise ratio. Since deuterated benzene was used as solvent, the main signal in ^{1}H NMR occurs from the protons of PS and the detected signal is conclusively classifiable as signal of the PS molecules. However, a slight signal occurring from the residual protonated solvent molecules ($C_6H_xD_y$, $x + y = 6$) was always detected. All measurements were performed at a temperature of 298 K with an accuracy of ± 1 K. The self-diffusivities were studied using an observation time Δ varying between 1 and 1000 ms. During the self-diffusion measurements, all samples showed no evidence of convection or flow. Measurements of several samples were repeated after about six months of storage and did not show significant changes in the measured diffusion parameters. To accurately calibrate the magnetic field gradient of the NMR spectrometer, self-diffusion measurements in pure H_2O done by Holz et al.[67] were used as reference. The given measurement uncertainties are composed of the direct measured uncertainty plus the fitting error uncertainty.

Results and Discussion

Figure 4 shows selected observation time-dependent spin echo attenuation curves of the PS/C_6D_6-loaded acrylate-based monoliths, which are representative for all concentrations and molar masses. All curves obtained can be approximated by using eq 3 for two diffusion regimes ($n = 2$). The self-diffusion coefficients

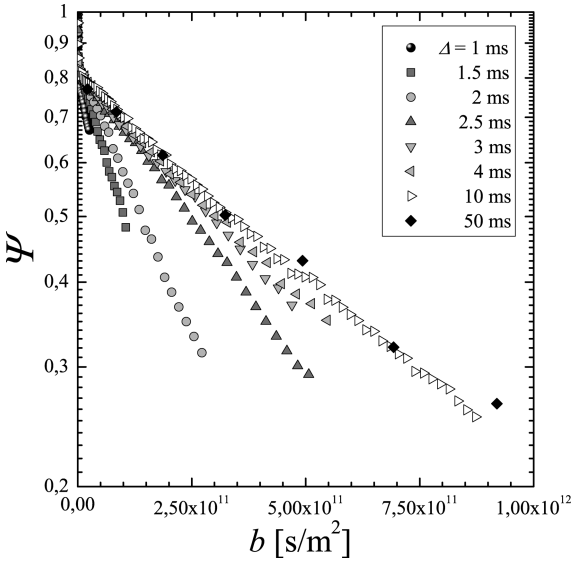

Figure 4. Semilogarithmic plot of the spin echo attenuations $\Psi(b)$ for different observation times Δ for PS dissolved in deuterated benzene soaked into the porous acrylate-based monoliths (M_{PS} = 864 000 g/mol, c_{PS} = 2 wt %).

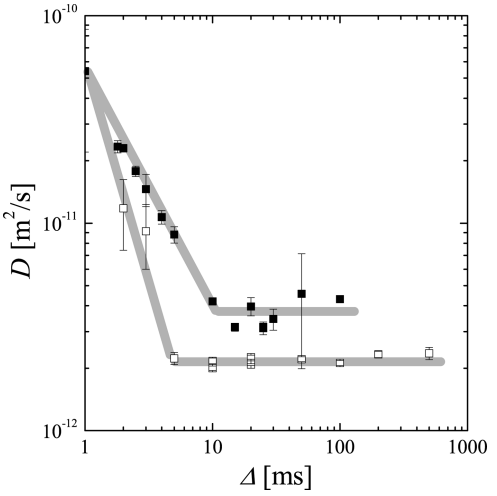

Figure 5. Double logarithmic plot of the observation time dependency of the self-diffusion coefficient of PS dissolved in deuterated benzene (M_{PS} = 601 800 g/mol, c_{PS} = 2 wt %) for the pure solution (■) and the solution soaked into the porous monoliths (□).

of the fast components are found to be in the order of about 10^{-9} m^2/s. This component can be attributed to the solvent self-diffusion, which is observed by ^{1}H NMR due to residual protons in the deuterated benzene. Its total amount is for all samples investigated lower than 15%. The slower component represents the collective self-diffusion of the PS chain system and is the point of interest in this study. In the displayed case of a molar mass of M_{PS} = 864 000 g/mol and a concentraion of c_{PS} = 2 wt %, the spin echo attenuation curves show no significant change for observation times exceeding about 10 ms. This behavior occures for the lowest molar masses (M_{PS} = 2600 g/mol) at observation times < 1 ms and for the highest molar masses (M_{PS} = 900 000 g/mol) at observation times of round about 20 ms.

Figure 5 displays the self-diffusion coefficients of the PS molecules dissolved in deuterated benzene (D_S) and of this PS solution soaked into the porous monoliths (D_M) in dependence on the observation time Δ. As one can see, with increasing time, the self-diffusion coefficient decreases until it saturates to a

constant value. Whereas for low observation times the internal motions and oscillation of the PS chains were detected, for longer times exceeding the above-mentioned time scales, the self-diffusion coefficient describes the collective motion of the PS chain system. Additionally, a faster decrease of the self-diffusion coefficient in the PS/C_6D_6-filled acrylate-based monoliths is observable, which is due to the interaction of the diffusing molecules with the inner surface of the porous material. For the chromatographic application of the porous acrylate-based monoliths, the collective self-diffusion coefficient is relevant. Therefore, the measured self-diffusion coefficients are compared at an observation time Δ exceeding 25 ms. To proof the adaptability of eq 1 in Figure 6, the mean square displacement of the PS molecules in parallel to the applied magnetic field gradient $\langle z^2(\Delta)\rangle$ is plotted on a double logarithmic scale against the observation time Δ. Generally, a slope of 1 is observed, which shows the direct proportionality of $D \propto \Delta$ and eq 1 is valid for the collective diffusive motion of the PS chains in the present case.

The extracted self-diffusion coefficients are shown in Table 1 and are plotted in Figure 7 as a function of the molar mass. The double logarithmic scale in Figure 7 provides the opportunity to extract the coefficient k of the characteristic dependency of the self-diffusion coefficient D on the molar mass M_{PS}:

$$D \propto {M_{PS}}^{k} \tag{4}$$

The lines in Figure 7 are representative to the diffusion data of the PS solutions in the porous monoliths. However, they are obviously also characterizing the molar mass dependence in the pure PS solutions, since their self-diffusion coefficients are found to be just a small factor larger than that of the PS solutions in the monoliths (see also Table 1).

In the molar mass dependence of the PS self-diffusion, a clear crossover from a characteristic exponent of $k \sim -0.5$ to higher values of -1.2 to -1.9 can be observed. This crossover occurs for all three concentrations at a molar mass of about 30 000 g/mol. This behavior agrees with corresponding data for pure solution of PS dissolved in toluene measured by fluorescence correlation spectroscopy recently published by Zettl et al.[10]

For concentrations smaller than 30 000 g/mol, the characteristic exponent of $k \sim -0.5$ agrees with the prediction of the Zimm-model,[68] which assumes diffusion of interacting individual polymer chains, which are not entangled. Within the experimental error it is also consistent with the model of diffusion in solutions below the overlap concentration,[1,2,10] which predicts $k = -0.6$.

At $M_{PS} > 30\,000$ g/mol and the highest concentration of 15 wt %, k is found to be -1.9 and thus, very close to the prediction of the Doi-Edwards (reptation) model for semidiluted entangled solution.[10,69,70] Therefore, $M_{PS} \approx 30\,000$ g/mol may be identified as the entanglement molar mass M_E. For the smaller concentrations (2 and 5 wt %), the characteristic exponent clearly exceeds the value for dilute, unentangled solution, but does not reach the value of $k = -2$. Therefore, we conclude that the PS chains are not yet fully entangled in this concentration range, since the concentrations are smaller than the overlap concentration.

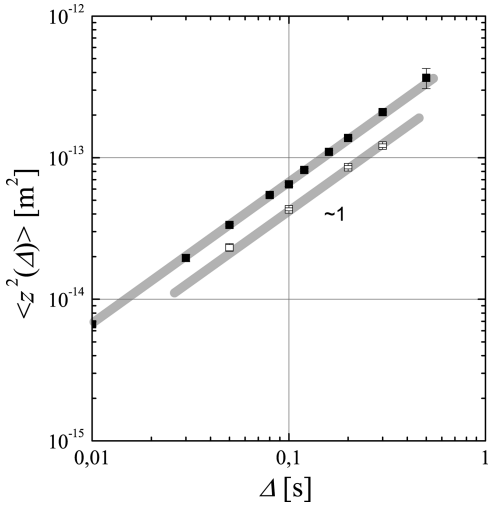

Figure 6. Double logarithmic plot of the measured mean square displacement $\langle z^2(\Delta)\rangle$ over the observation time Δ for the PS self-diffusion in deuterated benzene (■) and in deuterated benzene soaked into acrylate-based monoliths (□) (M_{PS} = 301 600 g/mol, c_{PS} = 15 wt %).

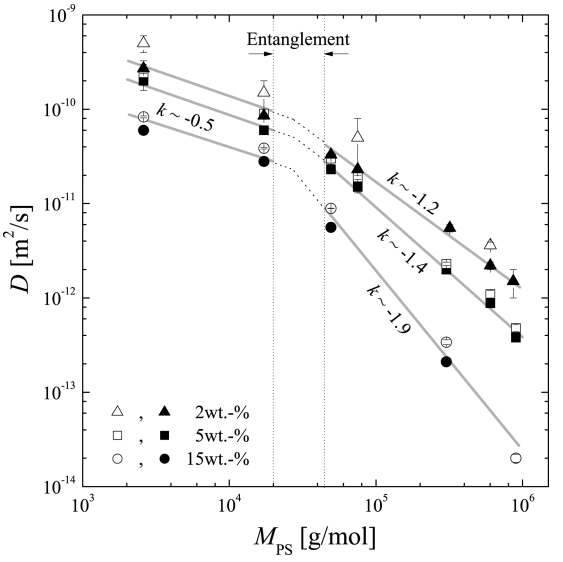

Figure 7. Double logarithmic representation of the self-diffusion coefficients D in dependence of the molar mass M_{PS} for the different concentrations of PS dissolved in deuterated benzene (open symbols) and of PS dissolved in deuterated benzene soaked into the porous monoliths (full symbols).

Table 1. Self-Diffusion Coefficients of Solutions of PS in C_6D_6 (D_S) and of PS in C_6D_6 Soaked into the Monolithic Materials (D_M)[a]

	2 wt %		5 wt %		15 wt %	
M_{PS} [g/mol]	D_S [m^2/s]	D_M [m^2/s]	D_S [m^2/s]	D_M [m^2/s]	D_S [m^2/s]	D_M [m^2/s]
2 600	$(5.0 \pm 0.5) \times 10^{-10}$	$(2.7 \pm 0.3) \times 10^{-10}$	$(2.4 \pm 0.4) \times 10^{-10}$	$(2.0 \pm 0.2) \times 10^{-10}$	$(8.3 \pm 0.2) \times 10^{-11}$	$(6.0 \pm 0.6) \times 10^{-11}$
17 200	$(1.5 \pm 0.3) \times 10^{-10}$	$(8.5 \pm 0.5) \times 10^{-11}$	$(0.9 \pm 0.1) \times 10^{-10}$	$(6.0 \pm 0.3) \times 10^{-11}$	$(3.9 \pm 0.1) \times 10^{-11}$	$(2.8 \pm 0.2) \times 10^{-11}$
49 300		$(3.3 \pm 0.2) \times 10^{-11}$	$(3.0 \pm 0.4) \times 10^{-11}$	$(2.3 \pm 0.1) \times 10^{-11}$	$(8.9 \pm 0.1) \times 10^{-12}$	$(5.6 \pm 0.2) \times 10^{-12}$
75 000	$(5.0 \pm 0.5) \times 10^{-11}$	$(2.3 \pm 0.1) \times 10^{-11}$	$(1.9 \pm 0.1) \times 10^{-11}$	$(1.5 \pm 0.2) \times 10^{-11}$		
301 600			$(2.3 \pm 0.1) \times 10^{-12}$	$(2.0 \pm 0.1) \times 10^{-12}$	$(3.4 \pm 0.2) \times 10^{-13}$	$(2.1 \pm 0.1) \times 10^{-13}$
319 000		$(5.5 \pm 0.5) \times 10^{-12}$				
601 800	$(3.6 \pm 0.3) \times 10^{-12}$	$(2.2 \pm 0.2) \times 10^{-12}$	$(1.1 \pm 0.1) \times 10^{-12}$	$(8.8 \pm 0.2) \times 10^{-13}$		
864 000		$(1.5 \pm 0.5) \times 10^{-12}$				
900 000			$(4.8 \pm 0.4) \times 10^{-13}$	$(3.8 \pm 0.3) \times 10^{-13}$	$(2.0 \pm 0.2) \times 10^{-14}$	

[a] The values were extracted from measurements performed at $\Delta > 25$ ms and represent the collective motion of the PS molecules.

Table 2. Necessary Pore Sizes for Getting Penetrated by a Certain PS Standard (Compare also Halász et al.[61,62])

M_{PS} [g/mol]	pore size [nm]
benzene	0.8
2 600	6.4
17 200	19.5
49 300	36.4
62 300	41.7
301 600	105.9
319 000	109.5
601 800	159.3
864 600	197.2
900 000	202.0

It should be noted again that our NMR measurements do not provide any evidence that the characteristic exponents for the molar weight dependences of the self-diffusion for the PS molecules in pure benzene solutions differ from the ones of the PS solutions in the porous acrylate-based monoliths. Therefore, the general trend and scaling laws, which are well established for polymer solutions, do also apply for the diffusion of the polymers through the pore space of these porous monoliths.

This finding may be rationalized by comparing the pore size distribution of the porous monoliths with the necessary pore size for getting penetrated by a certain PS standard,[61,62] which may be considered as the minimum pore size required in order to accommodate a PS molecule. As can be seen from Figure 2, the monoliths used contained pores <6 nm as well as pores in the range of 65−350 nm. Table 2 summarizes the minimum pore diameters that are necessary to be penetrated by a certain PS standard. From these values it becomes clear that none of the PS standards used can penetrate the pores <6 nm. This means that none of the PS standards penetrate the micro- or mesopores of the monoliths. However, all standards can at least in part penetrate the macroporous fraction, which is characterized by pores in the range of 65−335 nm. Moreover, the largest macropores are more than an order of magnitude wider than the maximum required pore sizes for getting penetrated by a certain PS standard given in Table 2. Therefore, even the PS molecules with the highest molar mass diffuse over short length scales as in the pure solutions.

The only pronounced difference between the PS self-diffusion in the pure solution (D_S) and in the monoliths (D_M) is a small reduction of the self-diffusion coefficients observed at sufficient long observation times (see Figures 5 to 7). Table 3 shows the calculated ratios of D_S/D_M for all molar masses and concentrations. Obviously, the ratio D_S/D_M does not depend on the molar mass of the diffusing molecules. In this case, the D_S/D_M ratio is identifiable with the tortuosity factor τ of the porous monoliths. It is defined as the squared ratio of the averaged effective pathway trough the pore space l_{eff} and the direct connection l of two points in the pore space of the porous material:[71,72]

$$\tau \equiv \left(\frac{l_{eff}}{l}\right)^2 \overset{eq1}{=} \frac{D_S}{D_M} \tag{5}$$

In the present case the investigated PS standards are not able to access the microporous regime of the monoliths. However, all investigated PS standards can penetrate the (same) macroporous space, which is the reason that we find a tortuosity factor which does not depend on the PS molecular mass. From the data in Table 3 one estimates a tortuosity factor averaged over all concentrations of about 1.5 ± 0.2.

This tortuosity factor strongly correlates with the initial turnover frequencies (TOF_0) found in the ring-closing metathesis (RCM) reaction of diethyl diallyl malonate catalyzed in solution by $Ru(CF_3COO)_2(IMesH_2)(CH\text{-}2\text{-}(2\text{-}PrO)\text{-}C_6H_4)$ (**1**) and by a

Table 3. Calculated Tortuosity $\tau = D_S/D_M$ for All Examined Molar Masses and Concentrations

M_{PS} [g/mol]	2 wt %	5 wt %	15 wt %
2 600	1.9 ± 0.4	1.2 ± 0.3	1.4 ± 0.2
17 200	1.8 ± 0.4	1.5 ± 0.2	1.4 ± 0.1
49 300		1.3 ± 0.2	1.6 ± 0.1
75 000	2.2 ± 0.3	1.3 ± 0.2	
301 600		1.2 ± 0.1	1.6 ± 0.2
601 800	1.6 ± 0.3	1.3 ± 0.1	
900 000		1.3 ± 0.2	
average	1.9 ± 0.3	1.3 ± 0.2	1.5 ± 0.2

monolith-immobilized analogueon, i.e. $Ru(monolith\text{-}CF_2CF_2COO)(CF_3COO)(IMesH_2)(CH\text{-}2\text{-}(2\text{-}PrO)\text{-}C_6H_4)$ (**2**). We chose this initial turnover frequency (TOF_0) as a measure, since TOF_0 can be calculated from the number of turnovers at a given time (short after the start of the reaction) per the initial number of catalytic centers. The latter can easily be determined, e.g., by inductively coupled optical emission spectroscopy (ICP-OES). The initial number of catalytic sites is the only valid measure since this number can decrease over time, e.g., by catalyst decomposition during the RCM reaction of a substrate, thereby changing the number of catalytic sites. From the data presented by Krause et al.[50] TOF_0 values of 0.21 s^{-1} for **1** and of 0.13 s^{-1} for **2** were calculated. Thus, the TOF_0 for the RCM reaction in solution is about 1.6 times larger than the TOF_0 found for the RCM in the solution placed inside the monolithic material. What we now propose is that the geometrical factor of a pore or a porous system, i.e., the tortuosity, in fact is related to or affects the macroscopic motion of substrates inside such a porous system under given conditions. Thus, a highly tortuous system would result in rather low diffusion coefficients and consequently into low reaction rates at the catalytic centers by the substrate molecules and a comparable poor removal of the product molecules there from. This would result in low TOFs and a low TOF_0 (as well as in low turnover numbers, since catalyst decomposition would dominate). Vice versa, monoliths with low tortuosity guarantee for a good accessibility of the catalytic sites. Since the diffusion of the PS standards in solution is about 1.5 times the value found in the porous system, the same might be anticipated for substrate molecules to the catalytic sites located in the same porous system. Consequently, transport to and from the catalytic sites must be in the same range, i.e., 0.66 (which is 1 over 1.5) times of the value found in solution. Since the catalytic sites are similar, they must have the same reactivity for a given substrate. In fact, the ratio of TOF_0 of the supported catalyst over TOF_0 found in solution is 0.62. Thus, the tortuosity factor is represented there as well and no additional reduction in the TOF_0 is observed with the supported catalyst. This is a result of the fact that the polymeric monolithic support itself is designed in a way that the catalysts are not located inside any micro- or mesopores but rather at the inner surface of the support that is exposed to the large transport pores in the micrometer regime. Consequently, all catalytic sites are easily accessible without the necessity for the educts and products to diffuse into or out of a porous system. Therefore, the TOF depends on diffusion and thus on tortuosity. The data presented here are to the best of our knowledge the first correlation of diffusivity data with the catalytic performance of a polymeric monolithic support.

Conclusion

The self-diffusion coefficients of PS dissolved in benzene and PS dissolved in benzene soaked into porous acrylate-based monoliths were measured using the pulsed field gradient NMR technique. These transport processes of liquid-filled pores in these porous media are of high interest because of their relevance to chromatography and chromatographic separations, respectively, as well to catalysis and membrane separation. We showed that

the scaling laws ($D \propto M_{PS}^{k}$) for molar masses lower than the entanglement molar mass M_E and as well as beyond this molar mass are represented by the Zimm model and the Doi−Edwards model of reptation, respectively. These models also describe the self-diffusion, if the PS solutions are soaked into the porous acrylate-based monoliths with a sufficient fraction of macropores. The ratio of the self-diffusion coefficients of PS solutions with respect to the PS solution soaked into the monoliths was found to be independent of the molar masses of the PS standards. It represents the tortuosity of the investigated monoliths. This tortuosity of the pore space is also reflected in the ratio between the initial turn over frequency of the ring-closing metathesis reaction of diethyl diallyl malonate by both a soluble and a polymeric monolith-supported metathesis catalyst.

Acknowledgment. We thank the International Research Training Group "Diffusion in Porous Materials" (DFG IRTG 1056/2) for financial support. M.R.B. thanks the *Deutsche Forschungsgemeinschaft* (DFG, Project Number BU-2174/1-2) for funding. Special thanks to A. Prager, IOM Leipzig, for the recording of the REM pictures and to L. Rosenkranz, IOM Leipzig, for carrying out the irradiation experiments.

References and Notes

(1) de Gennes, P.-G. *Scaling Concepts in Polymer Physics*, 1st ed.; Cornell University Press: New York, 1979.
(2) Doi, M.; Edwards, S. F. *The Theory of Polymer Dynamics*, 1st ed.; Oxford University Press: Oxford, U.K., 2007.
(3) Callaghan, P. T.; Pinder, D. N. *Macromolecules* **1980**, *13*, 1085–1092.
(4) Fleischer, G. *Polym. Bull.* **1983**, *9*, 152–158.
(5) von Meerwall, E. D.; Amis, E. J.; Ferry, J. D. *Macromolecules* **1985**, *18*, 260–266.
(6) Budtov, V. P. *Makromol. Chem.* **1986**, *188*, 2353–2370.
(7) Appel, M.; Fleischer, G.; Kärger, J. *Macromolecules* **1994**, *27*, 4274–4277.
(8) Grabowski, C. A.; Mukhopadhyay, A. *Macromolecules* **2008**, *41*, 6191–6194.
(9) Pollak, T.; Köhler, W. *J. Chem. Phys.* **2009**, *13*, 124905–124905−5.
(10) Zettl, U.; Hoffmann, S. T.; Koberling, F.; Krausch, G.; Enderlein, J.; Harnau, L.; Ballauff, M. *Macromolecules* **2009**, *41*, 9537–9547.
(11) Wesson, J. A.; Noh, I.; Kitano, T.; Yu, H. *Macromolecules* **1984**, *17*, 782–792.
(12) Deschamps, H.; Leger, L. *Macromolecules* **1986**, *19*, 2760–2765.
(13) Guo, Y.; O'Donohue, S. J.; Langley, K. H.; Karasz, F. E. *Phys. Rev. A* **1992**, *46*, 3335–3342.
(14) Zhou, Z.; Teraoka, I.; Langley, K. H.; Karasz, F. E. *Macromolecules* **1994**, *27*, 1759–1765.
(15) Teraoka, I.; Zhou, Z.; Langley, K. H.; Karasz, F. E. *Macromolecules* **1996**, *29*, 37–43.
(16) Beschieru, V.; Rathke, B.; Will, S. *Microporous Mesoporous Mater.* **2009**, *125*, 63–69.
(17) Christ, B. *J. Non-Crystalline Solids* **1991**, *131−133*, 709–714.
(18) Mukhopadhyay, R.; Mitra, S. *Indian J. Pure Appl. Phys.* **2006**, *44*, 732–740.
(19) Haas, O.-E.; Simon, J. M.; Kjelstrup, S.; Ramstad, A. L.; Fouquet, P. *J. Phys. Chem. C* **2008**, *112*, 3121–3125.
(20) Reeder, D. H.; Carr, P. W.; Flickinger, M. C.; McCormick, A. V. *J. Colloid Interface Sci.* **2000**, *226*, 277–285.
(21) Galvosas, P.; Stallmach, F.; Seiffert, G.; Kärger, J.; Kaess, U.; Majer, G. *J. Magn. Reson.* **2001**, *151*, 260–268.
(22) Stallmach, F.; Galvosas, P. *Annu. Rep. NMR Spectrosc.* **2007**, *61*, 51–131.
(23) Tennikova, T. B.; Belenkii, B. G.; Švec, F. *J. Liq. Chrom. Relat. Technol.* **1990**, *13*, 63–70.
(24) Belenkii, B. G.; Podkladenko, A. M.; Kurenbin, O. I.; Mal'tsev, V. G.; Nasledov, D. G.; Trushin, S. A. *J. Chromatogr.* **1993**, *645*, 1–15.
(25) Mal'tsev, V. G.; Nasledov, D. G.; Trushin, S. A.; Tennikova, T. B.; Vinogradova, S. V.; Volokitina, I. N.; Zgonnik, V. N.; Belenkii, B. G. *J. High Resolution Chromatogr.* **1990**, *13*, 185–189.
(26) Xie, S.; Švec, F.; Fréchet, J. M. J. *Biotechnol. Bioeng.* **1999**, *62*, 30–35.
(27) Švec, F.; Tennikova, T. B.; Deyl, Z. *Monolithic Materials: Preparation, Properties and Application.*, 1st ed.; Elsevier Science: Amsterdam, 2003.
(28) Buchmeiser, M. R. *Polymer* **2007**, *48*, 2187–2198.
(29) Sáfrány, A.; Beiler, B.; László, K.; Švec, F. *Polymer* **2005**, *46*, 2862–2871.
(30) Hosoya, K.; Hira, N.; Yamamoto, K.; Nishimura, M.; Tanaka, N. *Anal. Chem.* **2006**, *78*, 5729–5735.
(31) Tsujioka, N.; Hira, N.; Aoki, S.; Tanaka, N.; Hosoya, K. *Macromolecules* **2005**, *38*, 9901–9903.
(32) Nguyen, A. M.; Irgum, K. *Chem. Mater.* **2006**, *18*, 6308–6315.
(33) Sinner, F.; Buchmeiser, M. R. *Angew. Chem.* **2000**, *112*, 1491–1494.
(34) Sinner, F.; Buchmeiser, M. R. *Macromolecules* **2000**, *33*, 5777–5786.
(35) Bandari, R.; Knolle, W.; Buchmeiser, M. R. *Macromol. Rapid Commun.* **2007**, *28*, 2090–2094.
(36) Bandari, R.; Knolle, W.; Buchmeiser, M. R. *J. Chromatogr. A.* **2008**, *1191*, 268–273.
(37) Mayr, B.; Tessadri, R.; Post, E.; Buchmeiser, M. R. *Anal. Chem.* **2001**, *73*, 4071–4078.
(38) Buchmeiser, M. R. *Macromol. Rapid Commun.* **2001**, *22*, 1081–1094.
(39) Lubbad, S.; Mayr, B.; Huber, C. G.; Buchmeiser, M. R. *J. Chromatogr. A* **2002**, *959*, 121–129.
(40) Lubbad, S.; Buchmeiser, M. R. *Macromol. Rapid Commun.* **2002**, *23*, 617–621.
(41) Gatschelhofer, C.; Magnes, C.; Pieber, T. R.; Buchmeiser, M. R.; Sinner, F. M. *Chromatogr. A* **2005**, *1090*, 81–89.
(42) Lubbad, S.; Steiner, S. A.; Fritz, J. S.; Buchmeiser, M. R. *J. Chromatogr. A* **2006**, *1109*, 86–91.
(43) Bandari, R.; Prager-Duschke, A.; Kühnel, C.; Decker, U.; Schlemmer, B.; Buchmeiser, M. R. *Macromolecules* **2006**, *39*, 5222–5229.
(44) Schlemmer, B.; Gatschelhofer, G.; Pieber, T. R.; Sinner, F. M.; Buchmeiser, M. R. *J. Chromatogr. A* **2006**, *1132*, 124–131.
(45) Sinner, F.; Gatschelhofer, C.; Mautner, A.; Magnes, C.; Buchmeiser, M. R.; Pieber, T. R. *J. Chromatogr. A* **2008**, *1191*, 274–281.
(46) Mayr, M.; Mayr, B.; Buchmeiser, M. R. *Angew. Chem.* **2001**, *113*, 3957–3960.
(47) Mayr, M.; Mayr, B.; Buchmeiser, M. R. *Angew. Chem., Int. Ed.* **2001**, *40*, 3839–3842.
(48) Buchmeiser, M. R.; Lubbad, S.; Mayr, M.; Wurst, K. *Inorg. Chim. Acta* **2003**, *345*, 145–153.
(49) Krause, J. O.; Lubbad, S. H.; Nuyken, O.; Buchmeiser, M. R. *Adv. Synth. Catal.* **2003**, *345*, 996–1004.
(50) Krause, J. O.; Lubbad, S. H.; Nuyken, O.; Buchmeiser, M. R. *Macromol. Rapid Commun.* **2003**, *24*, 875–878.
(51) Mayr, M.; Wang, D.; Kröll, R.; Schuler, N.; Prühs, S.; Fürstner, A.; Buchmeiser, M. R. *Adv. Synth. Catal.* **2005**, *347*, 484–492.
(52) Beier, M. J.; Knolle, W.; Prager-Duschke, A.; Buchmeiser, M. R. *Macromol. Rapid Commun.* **2008**, *29*, 904–908.
(53) Rodrigues, A. E.; Zuping, L.; Loureiro, J. M. *Chem. Eng. Sci.* **1991**, *46*, 2765–2773.
(54) Bandari, R.; Knolle, W.; Prager-Duschke, A.; Buchmeiser, M. R. *Macromol. Chem. Phys.* **2007**, *208*, 1428–1436.
(55) Bandari, R.; Knolle, W.; Buchmeiser, M. R. *Macromol. Symp.* **2007**, *254*, 87–92.
(56) Bandari, R.; Elsner, C.; Knolle, W.; Kühnel, C.; Decker, U.; Buchmeiser, M. R. *J. Sep. Sci.* **2007**, *30*, 2821–2827.
(57) Rodrigues, A. E.; Ramos, A. M. D.; Loureiro, J. M.; Diaz, M.; Lu, Z. P. *Chem. Eng. Sci.* **1992**, *47*, 4405–4413.
(58) Rodrigues, A. E.; Loureiro, J. M.; Chenou, C.; de la Vega, M. R. *J. Chromatogr. A* **1995**, *664*, 233–240.
(59) Rodrigues, A. E. *J. Chromatogr. B* **1997**, *669*, 47–61.
(60) Rodrigues, A. E.; Mata, V. G.; Zabka, M.; Pais, L. *Flow and Mass Transfer*; Elsevier: Amsterdam, 2003.
(61) Halász, I.; Martin, K. *Angew. Chem.* **1978**, *90*, 954–961.
(62) Halász, I.; Martin, K. *Angew. Chem., Int. Ed.* **1978**, *17*, 901–908.
(63) Scheibitz, B.; Prager, A.; Buchmeiser, M. R. *Macromolecules* **2009**, *42*, 3493–3499.
(64) Stejskal, E. O.; Tanner, J. E. *J. Chem. Phys.* **1968**, *42*, 288–292.
(65) Kärger, J.; Bär, N. K.; Pfeifer, H.; Seiffert, G. *Z. Naturforsch.* **1995**, *50*, 186–190.
(66) Heink, W.; Kärger, J.; Seiffert, G.; Fleischer, G.; Rauchfuss, J. *J. Magn. Reson. A* **1995**, *114*, 101–104.
(67) Holz, M.; Heil, S. R.; Sacco, A. *Phys. Chem. Chem. Phys.* **2000**, *2*, 4740–4742.
(68) Zimm, B. H. *J. Chem. Phys.* **1956**, *24*, 269–278.
(69) Doi, M.; Edwards, S. F. *J. Chem. Soc., Faraday Trans. 2* **1978**, *74*, 1789–1801.
(70) de Gennes, P. G.; Léger, L. *Annu. Rev. Phys. Chem.* **1982**, *33*, 49–61.
(71) Stallmach, F.; Kärger, J. *Adsorption* **1999**, *5*, 117–133.
(72) Rigby, S.; Gladden, L. *J. Catal.* **1998**, *173*, 484–489.